

A MICROSCOPICALLY-INFORMED MODELLING APPROACH OF DAMAGE IN CEMENT-BASED MATERIALS

ABDERRAHMANE RHARDANE, SYED YASIR ALAM AND FREDERIC GRONDIN

Institut de Recherche en Génie Civil et Mécanique, GeM-UMR 6183, Centrale Nantes –

Université de Nantes – CNRS, 1 rue de la Noë, 44321 Nantes, FRANCE

e-mail: {abderrahmane.rhardane; syed-yasir.alam; frederic.grondin}@ec-nantes.fr, www.ec-nantes.fr

Key words: Damage, Cement paste, Mortar, Mesostructure, Multiscale, Particle Generation

Abstract: Multiscale modelling of damage in cementitious materials can be performed through either a downscale or an upscale approach. The drawback of downscale modelling is that it requires the recalibration of model parameters whenever the material composition changes. Therefore, an upscale approach is preferred. This article proposes a method of multiscale modelling of damage starting from the microscale. Once the intrinsic parameters of the cement paste phases are identified, the microscopically-informed modelling approach can theoretically be used for different concrete mixtures. The numerical simulations show that the transition from the scale of the cement matrix to the scale of mortar requires that the interfacial transition zone be modelled as a separate phase with different properties than the bulk matrix.

1 INTRODUCTION

The mesostructures of mortar or concrete are typically conceived as three-phase systems consisting of randomly generated aggregate particles embedded inside a binding cement matrix. The interfacial transition zone (ITZ) forming around aggregates is usually treated as a separate phase. In order to simulate damage, a damage model can be affected with fracture properties assigned to each of the phases. The properties of the binding cement matrix are conventionally calibrated through an inverse analysis scheme. While this method has been successfully used, it raises a few questions regarding the robustness of the procedure. In fact, the calibration of the model parameters at the mesoscopic scale requires the performance of experimental tests that can be burdensome and time-consuming. Moreover, the calibrated parameters need to be readjusted for each new mix design. On top of that, the lack of any assessment of the properties found at lower scales renders the approach less robust. Thus,

a calibration-free mesoscopic modelling of damage in cement-based materials calls for a microscopically-informed approach, taking into account the complex aspects of the hardening cement paste microstructure.

The first step of the simulation is the generation of the mesostructure. To construct the virtual mesostructure, a particle generation method is needed. Classical algorithms such as the take-and-place method [1]–[4], the divide-and-fill method [5], the random-extension and the random-walking algorithms [6], [7] suffer from a numerical sluggishness due to constant overlap-checking between placed particles. An easily-implemented algorithm addressing the weak points of the stated classical methods is proposed. The new algorithm can be 250 times faster than the commonly used take-and-place method [8].

In this article, the upscale approach is illustrated through the modelling of damage at the mortar scale. The approach can easily be extended to concrete. The new particle generation algorithm is first used to create the

mesostructure, which is composed of sand, cement paste and the ITZ. The fracture properties of the matrix are determined via an experimentally-validated simulation approach developed for the purpose of modelling complex phenomena such as creep, thermal cracking and freeze-thaw at the microscopic scale [8]. A parametric study is conducted with the aim of identifying the influence of the fracture properties of each phase. The numerical results show that failure to account for the interfacial zone leads to a constitutive behaviour for mortar that is as brittle as that of the cement paste. The simulations also demonstrate the important role of the ITZ properties on the global behaviour of mortar, and show that the ITZ must have a smaller tensile strength and higher fracture energy in order to account for the experimental results.

2 PRINCIPLES OF THE UPSCALING APPROACH

A concrete mesostructure (10^{-3} - 10^{-1} m) can be thought of as a three-phase material that is composed of coarse aggregates embedded in a mortar matrix with an interfacial transition zone, as illustrated in Figure 1. Mortar matrix (10^{-4} - 10^{-3} m) can in itself be decomposed into sand particles, an ITZ and a binding cement matrix. The bulk matrix (10^{-6} - 10^{-4} m) is a heterogeneous composite made of unhydrated particles (issued from clinker) ingrained in a matrix of different hydrates. To simulate the damage of these materials at each scale, a mesostructure is generated and then converted into a finite element mesh. A damage law is attributed to the phases, using parameters that are linked to phase properties. The properties of the binding matrices are determined at the lower scales. At the scale of cement paste, the damage behaviour depends entirely on the phase fractions and their arrangement within the microstructure, as the properties of each of these phases are considered intrinsic. Uniaxial tension and compression simulations can therefore be conducted to determine the macroscopic response of the cement paste, and this behaviour is then injected at the scale of mortar to the bulk cement matrix, and so forth.

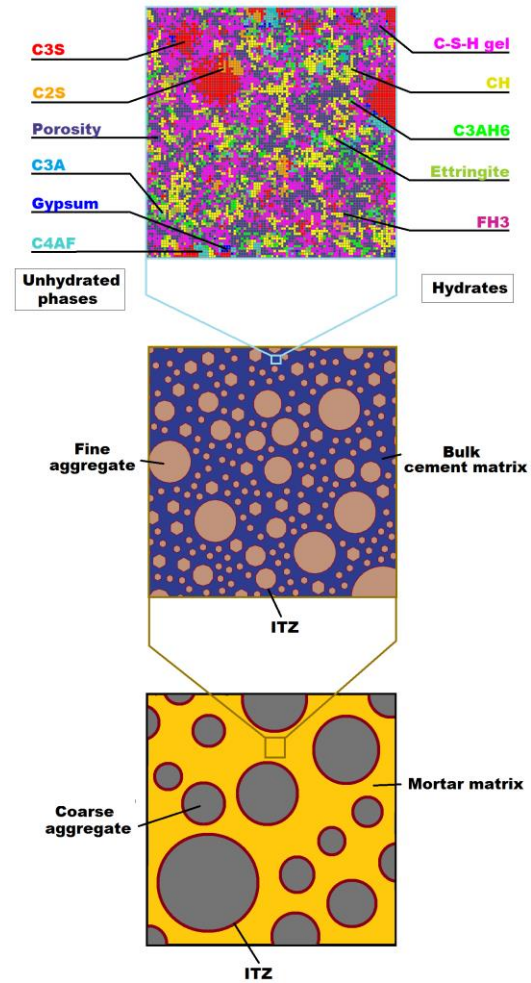


Figure 1: Multiscale modelling of concrete.

The principles of the upscaling approach can be described in the following manner:

- The mix composition is defined (i.e. type of cement, particle size distribution of clinker and additives, mix proportions, w/c ratio, curing conditions, volume fractions of fine and coarse aggregates, etc.).
- The virtual microstructure of cement paste is generated through a hydration model (the hydration platform VCCTL [9] is used in this case) and converted into a FE mesh.
- The damage law developed by Fichant [10], [11] and used for damage modelling of cement-based materials is adopted for all cement phases (a full description of the model and its application is given in [12]).
- The intrinsic micromechanical properties attributed to cement phases (elastic moduli, tensile strength and fracture energy) are used to calculate the parameters of the

damage model.

- Uniaxial tension and compression are simulated and the macroscopic stress-strain curve is calculated by volume averaging.
- The macro-properties of the homogenized cement paste are determined from the global response.
- The VCCTL hydration model is used once again to simulate the hydration of cement near a fixed boundary. This exemplifies the hydration evolution of the cement in the ITZ. The elastic properties are calculated using classical homogenisation methods.
- At the scale of mortar, the mesostructure is generated via the newly developed zone-of-influence method and converted into a FE mesh in in the finite element code Cast3M.
- Fichant's damage law is attributed to the phases of mortar. The properties are already determined at the microscale.
- Simulation of damage at the mesoscale is launched. In order to proceed to the level of concrete, uniaxial tensile and compressive tests can be simulated in order to determine the stress-strain curve of mortar, which can be used to determine the properties of the mortar matrix at the scale of concrete.

In this article, the study will be limited to the simulation of the three-point bending test at the mortar scale. The mortar composition studied in this example is composed of a class 0-4mm rolled river sand (44.7% of the mortar volume) and a type I Portland cement with a w/c ratio of 0.45. Three notched beams of 7x7x28cm in size are tested under three-point bending at the age of 28 days, and the F-CMOD curve is determined to compare the experimental data to the numerical results. The mix design is given in Table 1 and the F-CMOD curve is shown in Figure 2.

Table 1: Mix design of the studied mortar.

	Sand	CEM I 52.5 N	Effective water	Added water
Mass (kg/m ³)	1175.4	667.9	300.5	305.2
Density	2.63	3.12	1	1

Through this example, the first attempt is to use the upscaling approach to investigate

whether or not the damage of mortar can be entirely predicted from the behaviour of the phase components. Section 3 of this article deals with the numerical simulations leading to the determination of the cement paste macro-properties while in section 4, mortar is studied under three-point bending.

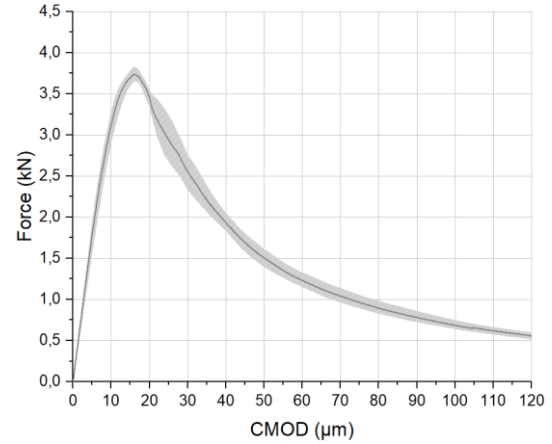


Figure 2: Experimental F-CMOD curve of mortar (thick line=average curve over three beams).

3 MACROSCOPIC PROPERTIES OF THE CEMENT PASTE AND THE ITZ

3.1 Properties of the bulk cement paste

The virtual microstructure of cement paste is first generated using the hydration model. The input parameters include the clinker composition ($C_3S=72.2\%$, $C_2S=9.4\%$, $C_3A=9.4\%$, $C_4AF=7.8\%$, $K\bar{S}=1.3\%$, $N\bar{S}=0.3\%$), the added gypsum (4.2%), the particle size distribution of cement (found using laser diffraction), the w/c ratio (0.45), the curing conditions (20°C, isothermal and sealed) and the cycle-time conversion curve (calculated from the isothermal calorimetry curve). All the input data are characteristic of the cement and the composition and do not require calibration. The microstructure at 28 days is extracted and converted into a FE mesh using the Cast3M FE code [13], as shown in Figure 3. The same damage law (Fichant et al.) is applied to all the phases, with only the damage parameters that vary from phase to phase.

In damage mechanics, the total stress σ is calculated from the effective stress $\tilde{\sigma}$ using a damage tensor. In the isotropic version of the

damage law mentioned above, the relationship can be written as:

$$\boldsymbol{\sigma} = (1 - D_T) \{\boldsymbol{\sigma}\}_+ + (1 - D_C) \{\boldsymbol{\sigma}\}_- \quad (1)$$

Where D_T and D_C are respectively the damage variables in tension and in compression. It is assumed that damage grows only due to tensile equivalent strains:

$$\varepsilon_{eq} = \sqrt{\sum \{\varepsilon_{ii}\}_+^2} \quad (2)$$

Where $\{\bullet\}$ are the Macaulay brackets. Given the following damage evolution law:

$$D_T = 1 - \frac{\kappa_0}{\varepsilon_{eq}} \exp\left[-B_T (\varepsilon_{eq} - \kappa_0)\right] \quad (3)$$

The damage parameters are linked to the phase properties (Young's modulus E , Poisson's ratio ν , tensile strength f_t and fracture energy G_f):

$$\begin{aligned} \kappa_0 &= \frac{f_t}{E} \\ B_T &= f_t \left(\frac{G_f}{h} - \frac{f_t^2}{2E} \right)^{-1} \end{aligned} \quad (4)$$

Therefore, the simulation at the microscale can be conducted once all the properties of cement phases are identified. Some of these properties have been determined using experimental and numerical techniques such as nanoindentation and molecular modelling. The elastic properties used in this study have been compiled from the literature. On the other hand, very few data can be found for the tensile strength and the fracture energy. The remaining properties have been determined using inverse analysis. First, the tensile strength and the fracture energy of a reference cement paste have been determined. Then, the microstructure corresponding to this cement paste is constructed and implemented in the FE code to simulate damage. The idea is to search for the micromechanical parameters of the phases that lead to the same properties of the cement paste that have been determined experimentally. The properties are therefore considered intrinsic to the phases. Table 2 shows the properties that are attributed to the main phases (a full list is available in [8]).

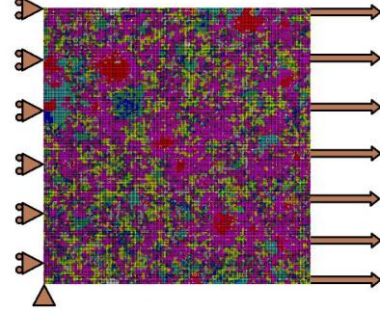


Figure 3: Microstructure of cement paste under tensile loading.

Table 2: Properties of the main cement paste phases.

Phase	E (GPa)	ν (-)	f_t (MPa)	G_f (J/m ²)
C ₃ S	137.4	0.30	430.7	65.8
C ₂ S	135.5	0.30	396.0	56.3
C ₃ A	145.2	0.28	534.6	94.3
C ₄ AF	150.8	0.32	470.3	72.5
Gypsum	44.5	0.33	29.6	0.98
CH	43.5	0.29	73.8	6.1
C-S-H	23.8	0.24	55.0	5.9
Ettringite	24.1	0.32	39.6	3.2
AFm	43.2	0.29	262.4	77.3

The REV of the cement paste is subjected to uniaxial tensile loading. Figure 4 shows the stress-crack opening displacement curve of the cement paste. The macroscopic properties are determined from this curve, with: $E=16$ GPa, $\nu=0.27$, $f_t=6.77$ MPa and $G_f=6.81$ J/m². The curve is then idealised to fit the description of the damage evolution law, as shown in Figure 4. At the mortar scale, the characteristic length h is taken as 200 μ m (the size of the REV).

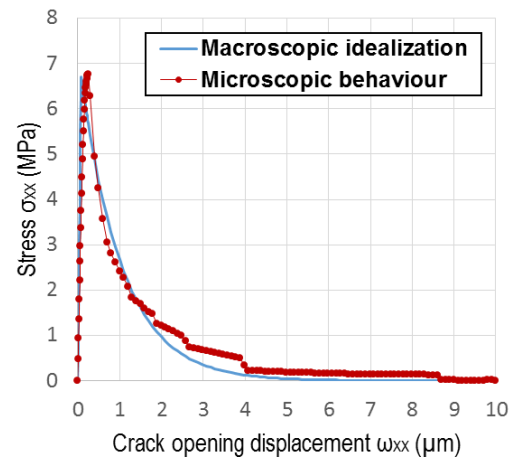


Figure 4: The stress-crack opening displacement curve of the cement paste (CEM I, $w/c = 0.45$).

3.2 Properties of the ITZ

The hydration model is used once again to simulate the evolution of the hydration near the surface of sand particle. Figure 5 illustrates the evolution of the Young's modulus and the Poisson's ratio within the ITZ, calculated using D-EMT [9]. The thickness of the ITZ is taken as $20\mu\text{m}$. To calculate the homogenized elastic moduli, the ITZ is subdivided into 10 layers and then homogenised as proposed in [14]. The effective elastic moduli are $E=14.81\text{GPa}$ and $\nu=0.279$. The difference obtained is explained by the porous nature of the ITZ, leading to a lower Young's modulus and a higher Poisson's ratio than the bulk cement paste.

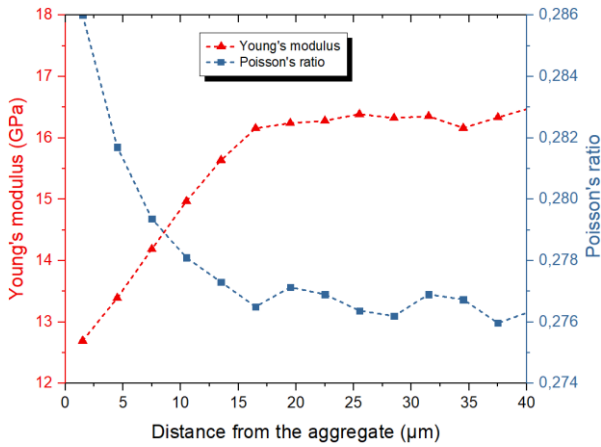


Figure 5: Evolution of the elastic moduli as a function of the distance from the sand inclusion.

4 MODELLING OF DAMAGE AT THE MESOSCOPIC LEVEL

4.1 Construction of the mesostructure

The virtual mesostructure of mortar can be idealised as a three-phase composite formed by sand inclusions, a binding cement matrix and an interfacial zone (ITZ). Unlike concrete, the volume fraction of inclusions in mortar is usually higher and the particle size is much smaller. This means that a significant number of particles must be placed inside the REV box. Classical algorithms such as the widely used take-and-place method require a huge amount of time to construct such REVs. To solve this, an improved particle generation algorithm is proposed. Figure 6 illustrates the following steps of the algorithm:

- First, the REV shape and size are defined and the particle size distribution of the sand is discretised into a number of classes (a).
- A feasible region is defined for each class. This region constitutes the set of all points where a particle's centre can be positioned. Initially, feasible regions take into account the boundary conditions of each class (b).
- Starting from the biggest class, a particle is placed randomly inside the RVE and the zone of influence is calculated. This area corresponds to the zone within which no particle can be placed, as it leads to overlap between particles (c).
- The next particle is placed randomly within the feasible region without the need for checking overlap. Once all the particles of one class are placed, the same procedure is repeated for the remaining classes (d-f).

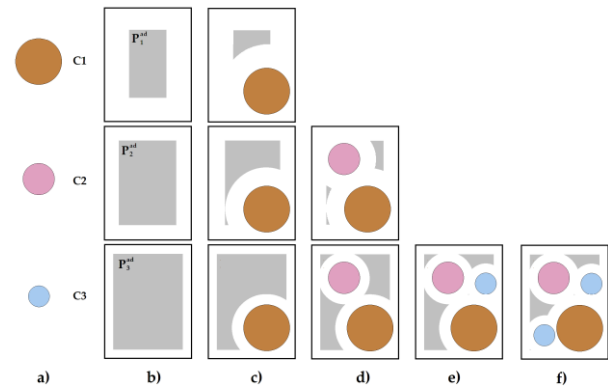


Figure 6: Construction of the mortar mesostructure using the sphere-of-influence algorithm.

The notched beam is modelled in Cast3M. For the sake of simplicity, only the central part (2cm in width) is meshed using a mesoscopic description (Figure 7). Using the proposed algorithm, the mesostructure can be generated in 6 minutes instead of 7 hours taken by the classical take-and-place method. The lateral parts have a macroscopic description to which an elastic behaviour is attributed.



Figure 7: Modelling of the mortar beam under three-point bending.

4.2 Simulation of damage: a parametric study

The properties of the phases of mortar are summed up in Table 3. The properties of the bulk cement paste and the ITZ have been determined in section 3.1 and 3.2, respectively. Sand inclusions are initially considered elastic and their properties are found in the literature. The elastic properties of the lateral parts are calculated using numerical homogenisation.

Table 3: Mechanical properties attributed to the phases of mortar.

Phase	E (GPa)	ν (-)	f_t (MPa)	G_f (J/m ²)
Bulk paste	16.0	0.27	6.77	6.81
Sand inclusions	78.0	0.20	-	-
ITZ	14.8	0.28	Unknown	
Lateral parts	29.6	0.23	-	-

The first series of the simulations (SIM0) does not take into account the presence of the ITZ. The calculated numerical F-CMOD curve is compared to the experimental curve (Figure 8). This comparison shows that the mortar is less resistant and more brittle than expected. An analysis of the crack propagation reveals that the main crack develops at the tip of the notch and advances inside the bulk matrix with no contribution from the aggregates. Affecting a damage behaviour to the sand particles with a variation of the strength (8 to 15MPa) and of the fracture energy (60 to 120J/m²) does not influence the global response of mortar. These results show the important role of the ITZ.

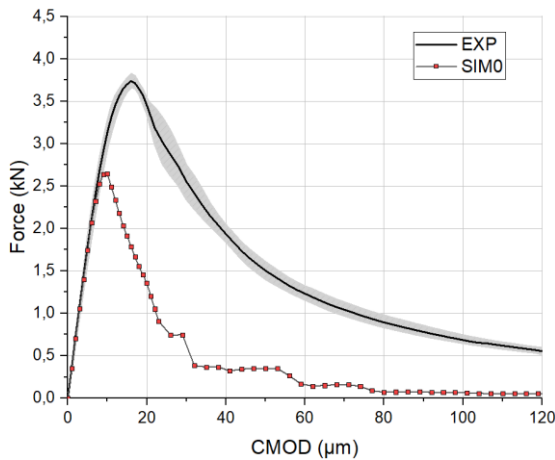


Figure 8: F-CMOD curve: absence of the ITZ.

The second series of the simulations take into account the explicit representation of the ITZ as a separate phase. The affectation of the same fracture properties of the bulk paste to the ITZ leads to the same behaviour described earlier. This means that the ITZ with its distinct properties is the main contributor to the crack arrest mechanisms. A parametric study is therefore conducted to investigate the influence of such properties. First, the tensile strength is fixed at 6.77MPa and the fracture energy is varied between 6.8J/m² and 120J/m². The results show that the influence is limited and the numerical F-CMOD curve is still far from the desired experimental curve (Figure 9). The crack profiles show that the increase is driven by the limited contribution of the ITZ's fracture energy when the crack passes along the interface. However, the main crack mostly advanced through the bulk cement paste. This is explained by the fact that the damage threshold of the ITZ is bigger than that of the bulk paste, since the elastic modulus is smaller (see Eq. 4).

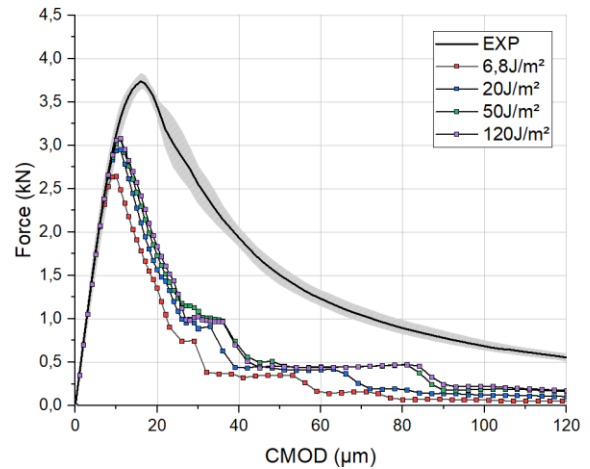


Figure 9: F-CMOD curve: influence of the ITZ's fracture energy ($f_t=6.77$ MPa).

For the third series of the simulations, the tensile strength is reduced to 6MPa to decrease the damage threshold of the ITZ. The fracture energy is again varied within the range 6.8-120J/m². The resulted F-CMOD curves, shown in Figure 10, show an important variation due to the contribution of the fracture energy to the global ductility of the material. The curves are closer to the experimental curve, but fall short

from of the desired behaviour even with high fracture energy (120J/m^2).

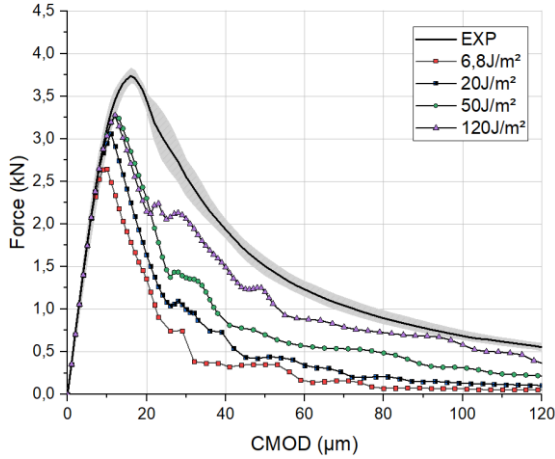


Figure 10: F-CMOD curve: influence of the ITZ's fracture energy ($f_t=6\text{MPa}$).

For the last series, the properties $f_t=6\text{MPa}$ and $G_f=120\text{J/m}^2$ are maintained for the ITZ. A size effect law is introduced to the behaviour of the sand particles linking the strength to the particle size between 1 and 4mm [15]:

$$f_{t,sand} \propto d_{sand}^{-0.35} \quad (5)$$

The obtained F-CMOD curve, shown in Figure 11, is very close to the experimental behaviour due to the contributions from the ITZ and the large sand particles which act as crack arrest mechanisms. A close investigation of the damage and the crack opening profiles (Figure 12) shows that the crack advances from the tip of the notch through the bulk and reaches a rather large sand inclusion. Damage grows inside and the main crack passes through the sand particle. The main crack then travels along the ITZ of smaller inclusions. Damage grows in the surroundings of the main crack. Occasionally, the crack is arrested due to the presence of a large sand particle or the high fracture energy of the ITZ, provoking the bifurcation of the main crack or forcing its deviation through the bulk cement paste.

Despite obtaining a numerical response of mortar that fits the experimental result and a cracking profile that is characteristic of the material, some questions can be raised relative to the high value found for the fracture energy of the ITZ. While it is true that the presence of

more porosity leads to arrest mechanisms and therefore a contribution to the total fracture energy, test simulations of a porous material with randomly distributed pores under tensile loading shows that the total fracture energy can only increase by a factor of 3. Therefore, the apparent quasi-brittleness of the mortar is unlikely to be explained by the high fracture energy of the ITZ, and more numerical and experimental tests are needed to demonstrate how to fully simulate the damage behaviour of quasi-brittle materials (mortar and concrete) which are composed of a more brittle material (cement paste).

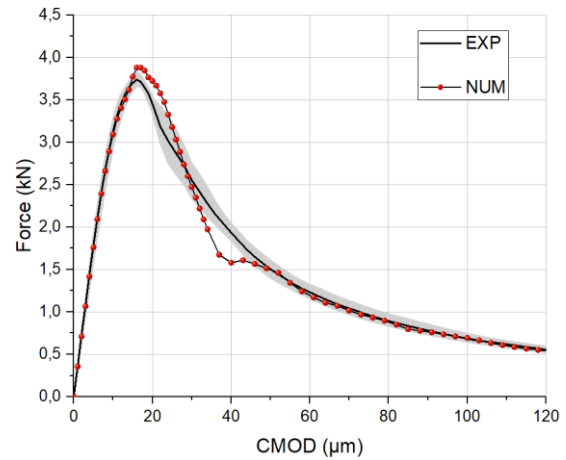


Figure 11: F-CMOD curve: attribution of a size effect law to the sand inclusions.

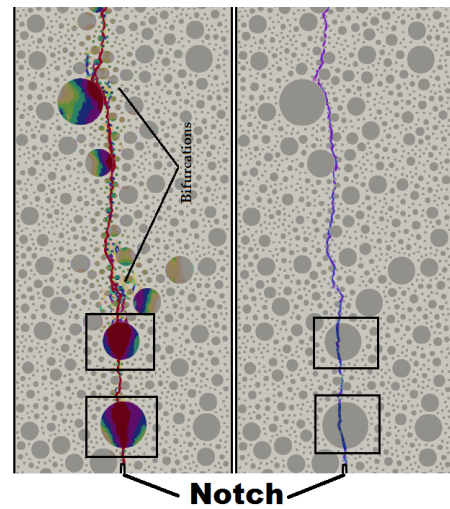


Figure 12: Evolution of the damage (left) and the crack opening (right) at the end of the simulation.

5 CONCLUSIONS

In this article, an upscaling modelling

approach of damage is suggested for cement-based materials. The main objective of this approach is to develop a scheme of modelling damage for different material compositions, without the need for new calibration of the model parameters.

The upscaling approach is used to simulate the fracture of mortar beams under three-point bending loads. Initially, the properties of all the mortar phases, including the bulk matrix and the ITZ, are determined at the microscale. The homogenised properties are then affected and used in a parametric study to investigate the influence of the properties of the ITZ. The numerical results show that failure to account for the ITZ leads to a brittle mortar. Results also show that the ITZ must have a low tensile strength and a high fracture energy to account for the experimental observations.

6 REFERENCES

- [1] Wittmann, F. H., Roelfstra, P. E., and Sadouki, H., 1985. Simulation and analysis of composite structures *Materials Science and Engineering* 68:239–248.
- [2] Bažant, Z. P., Tabbara, M. R., Kazemi, M. T., and Pijaudier-Cabot, G., 1990. Random Particle Model for Fracture of Aggregate or Fiber Composites *Journal of Engineering Mechanics* 116:1686–1705.
- [3] Schlangen, E. and van Mier, J. G. M., 1992. Simple lattice model for numerical simulation of fracture of concrete materials and structures *Materials and Structures* 25:534–542.
- [4] Grondin, F., Dumontet, H., Ben Hamida, A., and Boussa, H., 2011. Micromechanical contributions to the behaviour of cement-based materials: Two-scale modelling of cement paste and concrete in tension at high temperatures *Cement and Concrete Composites* 33:424–435.
- [5] De Schutter, G. and Taerwe, L., 1993. Random particle model for concrete based on Delaunay triangulation *Materials and Structures* 26:67–73.
- [6] Du, C., Sun, L., Jiang, S., and Ying, Z., 2013. Numerical Simulation of Aggregate Shapes of Three-Dimensional Concrete and Its Applications *Journal of Aerospace Engineering* 26:515–527.
- [7] Zhang, Z., Song, X., Liu, Y., Wu, D., and Song, C., 2017. Three-dimensional mesoscale modelling of concrete composites by using random walking algorithm *Composites Science and Technology* 149:235–245.
- [8] Rhardane, A., Élaboration d'une approche micromécanique pour modéliser l'endommagement des matériaux cimentaires sous fluage et cycles de gel-dégel, Ecole Centrale de Nantes, 2018.
- [9] Bullard, J. W. and Stutzman, P. E., 2006. Analysis of CCRL Portland Cement Proficiency Samples Number 151 and Number 152 Using the Virtual Cement and Concrete Reference Laboratory *Cem. Concr. Res.* 36:1548–1555.
- [10] Fichant, S., Pijaudier-Cabot, G., and La Borderie, C., 1997. Continuum damage modelling: Approximation of crack induced anisotropy *Mechanics Research Communications* 24:109–114.
- [11] Fichant, S., La Borderie, C., and Pijaudier-Cabot, G., 1999. Isotropic and anisotropic descriptions of damage in concrete structures *Mechanics of Cohesive-frictional Materials* 4:339–359.
- [12] Matallah, M., Farah, M., Grondin, F., Loukili, A., and Rozière, E., 2013. Size-independent fracture energy of concrete at very early ages by inverse analysis *Engineering Fracture Mechanics* 109:1–16.
- [13] Verpaux, P., Charras, T., and Millard, A., CASTEM 2000 une approche moderne du calcul des structures, *Calcul des structures et intelligences artificielle, Pluralis*, 1988. [Online]. Available: <http://www-cast3m.cea.fr>.
- [14] Grondin, F. and Matallah, M., 2014. How to consider the Interfacial

Transition Zones in the finite element modelling of concrete? *Cement and Concrete Research* 58:67–75.

- [15] Ovalle, C., Frossard, E., Dano, C., Hu, W., Maiolino, S., and Hicher, P.-Y., 2014. The effect of size on the strength of coarse rock aggregates and large rockfill samples through experimental data *Acta Mechanica* 225:2199–2216.